


 CrossMark
click for updates

Cite this: DOI: 10.1039/c6ce00365f

Chemical engineering of donor–acceptor liquid crystalline dyads and triads for the controlled nanostructuring of organic semiconductors†

 Yiming Xiao,^a Xiaolu Su,^a Lydia Sosa-Vargas,^a Emmanuelle Lacaze,^b
Benoît Heinrich,^c Bertrand Donnio,^{*c} David Kreher,^a
Fabrice Mathevet^{*a} and André-Jean Attias^{*a}

Multi-segregated columnar structures provide a geometrically ideal scheme for ambipolar organic semiconductors, but are not easy to design. A set of novel materials with dyad and triad architectures based on 2 different discotic cores is reported and the conditions of emergence of such complex structures are investigated. The designed molecules associate together electron-donor triphenylene cores (D) and perylene or naphthalene diimides as acceptor moieties (A), both entities being linked *via* alkyl chain spacers. The evaluation in solution of their HOMO/LUMO energy levels by cyclic voltammetry demonstrates the preservation of the individual features of the D and A units. Their thermal and self-organization behaviors were studied by polarized-light optical microscopy, differential scanning calorimetry, temperature-dependent small-angle X-ray scattering and dilatometry, which permitted detailed investigation of the self-organization behaviour. These D–A compounds turned out to spontaneously self-organize into columnar mesophases at room temperature, with the D and A moieties segregated into either alternated stacks within mixed columns or in distinct columns, the latter providing an ideal configuration for 1D hole and electron transport pathways. In view of potential applications of the triad/dyad template, thin films of these self-organized materials were also probed by atomic force microscopy and grazing incidence X-ray scattering.

 Received 12th February 2016,
Accepted 29th April 2016

DOI: 10.1039/c6ce00365f

www.rsc.org/crystengcomm

Introduction

The control of supramolecular self-assemblies and the nano-scale morphologies of π -conjugated architectures in organic semiconducting thin films can be seen as a critical issue for the improvement of device performance in the field of organic optoelectronics.¹ More particularly, the realization of nanostructured 3D morphologies of different types of electroactive constituents such as electron donor (D) or electron acceptor (A) building blocks is of great interest for organic solar cell (OPV) and for ambipolar organic field effect transistor (OFET) applications based on bulk heterojunction thin films.²

Indeed, these nanostructured morphologies offer the possibility to spontaneously form separate conduction pathways for hole and electron charge carriers, consequent to the antagonistic chemical nature of each building block. This condition is, however, not sufficient and optimal charge transport properties also imply the formation of appropriate long-range correlated structures with defined orientations and the ultimate control of the regular pathway alternation.

A common strategy is based on the elaboration of conjugated D–A block copolymers, which show the ability to undergo phase separation into well-ordered cylindrical or lamellar morphologies with periodicities ranging from the tens to hundreds of nanometers scale.³ However, these morphologies turn out to be difficult to realize and require fine tuning of the block structures and lengths.

As an alternative route toward D–A nanostructured 3D morphologies, the semiconducting architectures can be fitted with liquid crystalline properties.⁴ Liquid crystals are indeed outstanding examples of soft self-assemblies that combine order and fluidity, within components self-organizing into a wide diversity of long-range ordered and periodic structures.⁵ In addition, liquid crystal assemblies can form thin films which are intrinsically self-healing since structural defects are corrected automatically during the process of self-assembly.

^a Institut Parisien de Chimie Moléculaire (IPCM), Chimie des Polymères, Sorbonne Université, UPMC Université Paris 06, UMR 8232, F-75005 Paris, France.

E-mail: fabrice.mathevet@upmc.fr, andre-jean.attias@upmc.fr

^b Institut des NanoSciences de Paris (INSP), CNRS-Université Pierre et Marie Curie, UMR 7588, 4 Place Jussieu, 75005 Paris, France

^c Institut de Physique et Chimie des Matériaux de Strasbourg (IPCMS), CNRS-Université de Strasbourg, UMR 7504, F-67034 Strasbourg, France.

E-mail: bertrand.donnio@ipcms.unistra.fr

† Electronic supplementary information (ESI) available: Synthetic schemes, experimental procedures and chemical characterization of compounds, detailed polymorphic data, DSC, SAXS in the pristine state and at higher temperature, indexation tables of SAXS patterns of TPT, dilatometric curve of T, and GIXS in the as prepared state of TP. See DOI: 10.1039/c6ce00365f

Last but not least, the large variety of available π -conjugated mesogens allows the accurate tuning of the electronic and transport properties of the material through the control of the segregation at the molecular level.⁶

Among the large diversity of such π -conjugated mesomorphic building blocks, the disk-shaped ones involved in discotic liquid crystals (DLCs) are of particular interest.⁷ Consisting of a large π -conjugated polycyclic aromatic core peripherally equipped with several alkyl chains, DLCs give rise to phases in which the cores stack into columns producing an efficient 1D conductive pathway, whereas the surrounding flexible alkyl chains play the role of soft insulators between adjacent columns.

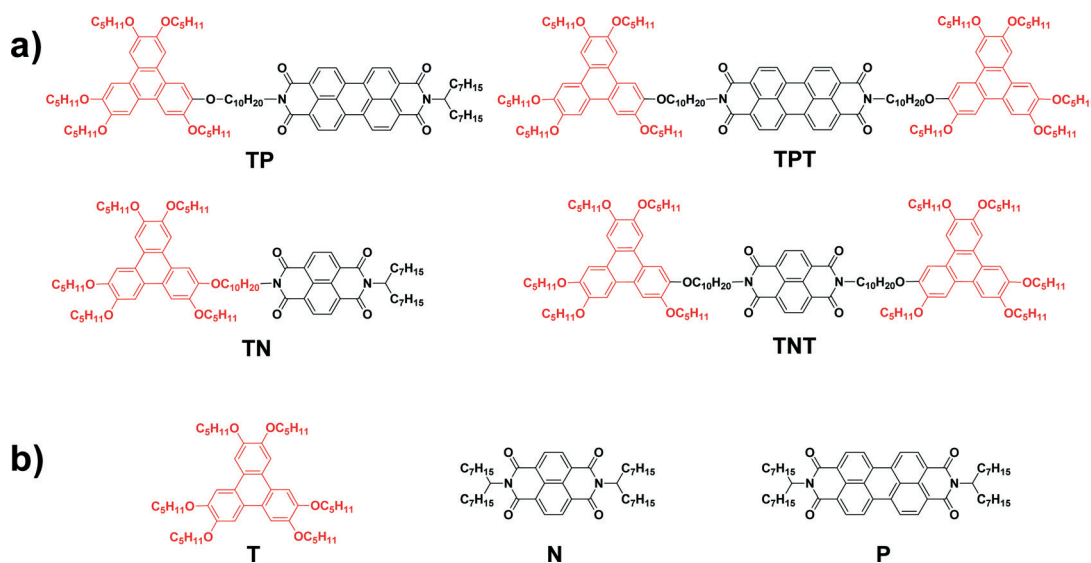
Triphenylene and rylene diimide derivatives are archetypal p-type (D) and n-type (A) DLCs, respectively, and each one has extensively been studied for its charge transport and photovoltaic properties.^{8,9} Nevertheless, only a few examples of D–A mesomorphic molecular architectures based on the combination of these entities have been reported until now, and none of them give rise to self-organized structures with long-range segregation between the D and A pi-fragments.^{4c,e} Zhao *et al.* in that regard very recently reported combined triphenylene and perylenediimide or coronenediimide moieties into D–A–D triad-type systems, which were found to self-organize in a lamello-columnar mesophase giving distinct p and n conducting channels through regular alternation of two disrupted rows of triphenylene columns and one continuous row of diimide species. The same favorable lamello-columnar self-organization was also found for the three triads, in relation to the side-connection through the short spacers of the rylene in the D–A–D architecture.¹⁰

In the same line, end-connection by the tip through a longer spacer would split the continuous rylene row and possibly yield true columnar mesophases, although the preservation of the mesomorphic properties is not straightforward.¹¹ Co-

lumnar self-organization might even represent a more favorable alternative to lamello-columnar phases, since both types of stacked species would then alternate in all directions of the lattice plane. With this highest degree of intermingling of conducting channels, the number of excitons photo-generated close to the large inter-column donor–acceptor interface and the conduction along the 1D hole and electron transport pathways would be optimum. To the best of our knowledge, such an ideal configuration for efficient formation of excited charge transfer states and good ambipolar charge carrier mobilities has never been realized so far, as indeed the emergence of such multi-segregated columnar structures is not trivial.

In this context, novel dyad and triad D–A mesomorphic materials based on discotic triphenylene and rylene diimide fragments were synthesized and investigated for the possible emergence of multi-segregated columnar structures. The family of molecules presented hereafter associates electron-donor triphenylene cores and rylene diimides as acceptor moieties, both entities being linked *via* alkyl chain spacers (Scheme 1a). The four compounds involve either a perylene or a naphthalene fragment, since both are recognized n-type DLCs with similar semiconducting properties but with different geometries, which determine the mesomorphism. We demonstrated that three of these D–A compounds turned out to spontaneously self-organize into columnar mesophases at room temperature, with the D and A moieties segregated into either distinct columns or in alternated stacks within mixed columns.

All the D–A systems were fully characterized by NMR and standard techniques. Their electronic properties, and more particularly their HOMO/LUMO energy levels, were evaluated by cyclic voltammetry to show the potential of these materials as ambipolar materials. Their thermal and self-organization behaviors were further investigated by polarized-light optical



Scheme 1 Chemical structures of a) the various targeted D–A mesomorphic dyads and triads and b) the individual model compounds: triphenylene T, naphthalene N and perylene P.

microscopy (POM), differential scanning calorimetry (DSC), temperature-dependent small-angle X-ray scattering (SAXS) and dilatometry, which permitted deep investigation of the self-organization behavior. In view of potential applications of the triad/dyad template, thin films of these self-organized materials were moreover probed by atomic force microscopy (AFM) and grazing incidence X-ray scattering (GIXS) to address alignments on the substrate surface.

Results and discussion

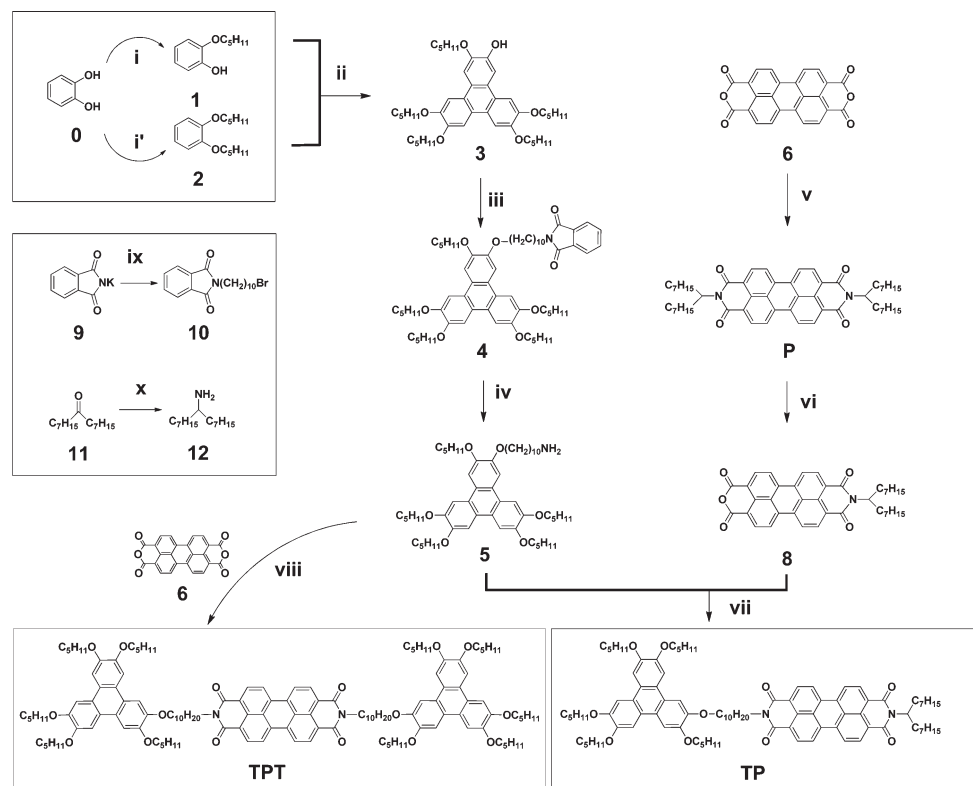
Synthesis

The D–A dyad **TP** and D–A–D triad **TPT** were prepared as depicted in Scheme 2. Whatever the target molecule is, the key intermediate is the triphenylene core bearing a single alkoxyamine side chain **5** prepared from the monohydroxy-pentaalkoxytriphenylene **3** (see the ESI†).¹² The unsymmetrical triphenylene **3** was alkylated with the building block **10** bearing a “pre-Gabriel” functional group to form the intermediate **4** which was deprotected with an ethanolic hydrazine solution to give the expected triphenylene amine **5**. For the synthesis of the dyad **TP**, the asymmetrically substituted monoimide perylene **8** was prepared according to Thelakkat's procedure¹³ based on the cleavage of one terminal branched

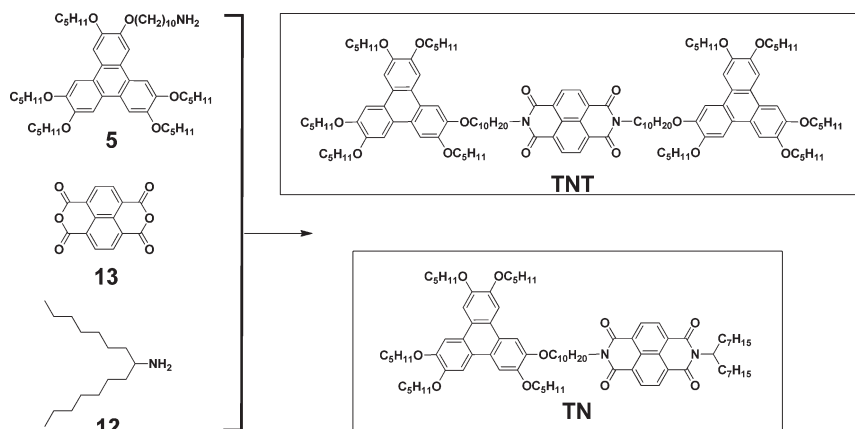
chain of the symmetrical diimide derivative **P** by partial saponification under strong basic conditions. Finally, the coupling between **5** and **8** by imidification reaction in melted imidazole, catalyzed by zinc acetate (Lewis acid) according to the literature procedure¹⁴ leads to the dyad in 75% yield. Similarly, the triad **TPT** is obtained by coupling the triphenylene amine **5** with the commercially available 3,4,9,10-perylene tetracarboxylic dianhydride **6**.

Concerning the D–A dyad **TN** and D–A–D triad **TNT** homologues based on the naphthalene acceptor unit, the previous strategy developed for the perylene-based compounds could not be applied. Indeed, our attempts to prepare the mono-anhydride mono-imide naphthalene derivative failed. The mono-imidification from 1,4,5,8-naphthalenetetracarboxylic dianhydride (NTCDA) did not work, and the mono-cleavage from the symmetric diimide naphthalene was also not possible. Thus, we developed a strategy based on a statistical approach, as described in Scheme 3. The imidification of NTCDA was eventually performed in one-pot by adding the two amine derivatives **5** and **12** in a 1 : 1 ratio. This way, the dyad **TN** and triad **TNT** were obtained in acceptable yields after easy purifications.

The model compounds **T**,¹⁵ **N**¹⁶ and **P**¹³ (Scheme 1b) were also prepared.



Scheme 2 Synthesis of D–A dyad **TP** and D–A–D triad **TPT** based on triphenylene and perylene cores. Reagents and conditions: *i*) 1-bromopentane (feeding ratio 2 : 1 to catechol), K_2CO_3 , KI, tetrabutylammonium bromide, EtOH, reflux, 24 h, 83%; *i'*) under the same conditions as *i'* with a feeding ratio of 1 : 1 with catechol, 79%; *ii*) $FeCl_3$, DCM/MeCN, 0 °C, 2 h, 22%; *iii*) **10**, K_2CO_3 , DMF, 120 °C, 12 h, 82%; *iv*) aqueous hydrazine hydrate, EtOH, reflux, 1.5 h, quantitative; *v*) **12**, $Zn(OAc)_2$, imidazole, 160 °C, 2 h, 81%; *vi*) KOH, *t*-BuOH, reflux, 1.5 h; AcOH; HCl, 43%; *vii*) $Zn(OAc)_2$, imidazole, 160 °C, 2 h, 75%; *viii*) $Zn(OAc)_2$, imidazole, 160 °C, 2 h, 45%; *ix*) 1,10-dibromodecane, DMF, 100 °C, 2 h, 72%; *x*) NH_2OH , EtOH, pyridine, 100 °C, 2 h; RedAl, toluene, reflux, 2 h, quantitative.



Scheme 3 Synthesis of D–A dyad TN and triad TNT based on triphenylene and naphthalene cores. Reagents and conditions: Zn(OAc)₂, imidazole, 160 °C, 2 h, TN 33%, TNT 20%.

The full synthetic and characterization details of TP, TPT, TN, TNT, T, N and P are reported in the ESI†

Electrochemical behavior and HOMO/LUMO energies

The electrochemical behaviors of TP, TPT, TN and TNT were investigated by cyclic voltammetry, the optimized experimental conditions being obtained with chloroform solutions (10^{−3} M) and by using 0.5 M *n*-Bu₄NPF₆ as the electrolyte. As an example, the cyclic voltammogram (CV) of TP is reported in Fig. 1.

In reduction, the voltammogram of TP shows two well-separated and reversible one-electron reduction waves at −0.67 and −0.86 V (vs. Ag/AgCl) related to the formation in the perylene acceptor moiety of the radical anion and dianion, respectively. In oxidation, a unique one-electron oxidation wave corresponding to the signature of the triphenylene donor moiety radical cation at 1.03 V (vs. Ag/AgCl) is evidenced. The other derivatives TPT, TN and TNT

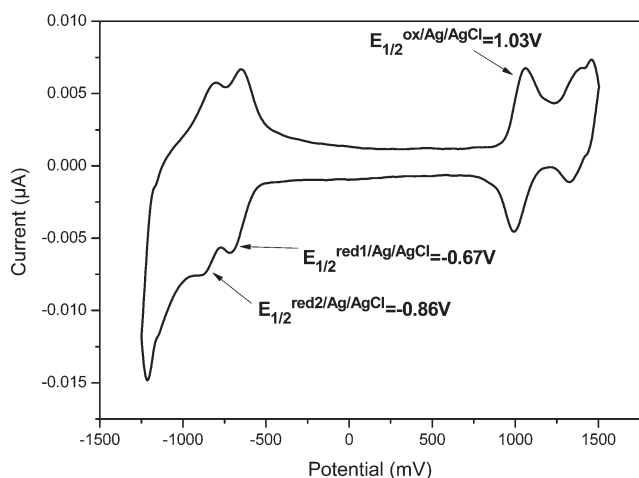


Fig. 1 Cyclic voltammetry (deconvoluted signal) of dyad TP in a chloroform solution (10^{−3} M) including 0.5 M *n*-Bu₄NPF₆. The experiment was carried out at a rate of 0.05 V s^{−1} at room temperature.

present similar electrochemical behaviors (see their CVs in Fig. S1†), which allowed us to determine their redox potential values. They are listed in Table S0 (ESI†).

Based on their redox potentials, the HOMO/LUMO energy levels of the four molecules can be calculated by using the following classical semi-empiric equations: estimated electron affinity (EA) or LUMO energy level, $E^{LUMO} = -(4.8 + E_{1/2}^{red1} \text{ (vs. Fc)})$ and estimated ionized potential (IP) or HOMO energy level, $E^{HOMO} = -(4.8 + E_{1/2}^{ox1} \text{ (vs. Fc)})$.¹⁷ Their values are summarized in Table 1. The estimated electron affinity (EA) or E^{LUMO} values are in the range of −3.77 to −3.87 eV for TP and TPT and −3.73 to −3.75 eV for TN and TNT, indicating that for a perylene dyad/triad, the LUMO energies are determined mainly by the LUMO energy of the perylene moiety (−4.1 eV for the P model compound), and for the naphthalene dyad/triad derivatives, the LUMO energies are governed by the LUMO energy value of the naphthalene moiety (−3.41 eV for the N model compound). Moreover, the estimated ionization potential (IP) or E^{HOMO} values are in the range of −5.43 to −5.47 eV for the four derivatives, indicating that these HOMO values are mainly the HOMO value reported for the triphenylene moiety T (−5.4 eV), under the same experimental conditions.

As a consequence, through comparison of all the reported HOMO–LUMO values in Table 1, we can conclude that the donor and acceptor units in this series of dyads and triads do not interact with each other and that the connection of the segments through the aliphatic spacers is a way to force their juxtaposition and preserve their genuine electronic properties.

Table 1 HOMO/LUMO energy levels of TP, TPT, TN and TNT

	TP	TPT	TN	TNT	T ^a	N ^a	P ^a
E^{HOMO} (eV)	−5.47	−5.43	−5.46	−5.45	−5.4	−7.04	−6.3
E^{LUMO} (eV)	−3.77	−3.87	−3.75	−3.73	−1.7	−3.41	−4.1
E_g^{CV} (eV)	1.7	1.56	1.71	1.72	3.7	3.63	2.2

^a The HOMO/LUMO values of model compounds T,¹⁸ N,¹⁹ and P^{9d} are published in the previous reports.

Characterization of the self-organization behavior

Although the triad/dyad architectures follow the electronic and molecular properties of the constitutive acceptor/donor segments, the separation of the latter in juxtaposed domains is also required for the expression of the D–A couple properties in the final material. The different natures of the segments should intrinsically initiate distinct self-aggregation processes, while the appropriate design of the interconnection and of a peripheral chain would ultimately lead to the coveted juxtaposition of different domains isolated from each other by a continuum of aliphatic chains. This molecular design naturally leads to self-organization in mesophases, which were first investigated by POM and DSC (results summarized in Table S1[†]), prior to deeper structural characterization by SAXS.

As evidenced by POM, except the dyad TN which is an isotropic liquid at room temperature, the other triads/dyad, TNT, TP and TPT, are soft solids at room temperature and gradually liquefy at higher temperature leading to birefringent fluid textures typical of a mesophase, which are maintained until the transition to the isotropic liquid, above 170 °C (TNT) or at 145–150 °C (TP and TPT). On cooling of the isotropic liquid, TNT and TP display pseudo focal-conic and dendritic textures, typical of columnar mesophases, while unconventional dendritic textures indicative of low symmetric structures are observed for TPT (Fig. 2). No textural changes occur on further cooling and the samples therefore exhibit a single mesophase, as also confirmed by the DSC traces that only display the isotropization peak (Fig. 2 and S2[†]). In particular, crystalline states are not observed for these compounds at low temperature, but the mesophases gradually freeze in an anisotropic glassy state between *ca.* 80 °C and room temperature, the transitional range being detectable as a slope change in DSC runs at a high heating rate. In contrast, the non-mesomorphic TN rigidifies into amorphous glass at a substantially lower temperature

(*ca.* –10 °C), by undergoing a sudden transition even visible at a low rate. The stiffening occurs in this case within a few degrees, as classically observed for organic liquids. For the mesomorphic analogues, the process is anticipated at higher temperatures and spread over tens of degrees, which means that the collective motions responsible for the fluidity are hindered by the molecular organization.

Hexakis(pentyloxy)-triphenylene, which is a representative of the “T” unit in triads and dyads, is crystalline at room temperature and melts at 65 °C to a Col_{hex} phase formed by the stacking of the triphenylene rings into columns and by the melting of peripheral chains in a continuum.²⁰ This structure is demonstrated in the SAXS patterns by the presence of the scattering signals $h_{\pi} \approx 3.5 \text{ \AA}$, arising from the face-to-face stacked rings, and $h_{\text{ch}} \approx 4.5 \text{ \AA}$, associated with the lateral distances between molten chains, in addition to the series of sharp reflections of the hexagonal lattice, namely the very strong first order ($d_{10} = 17.6 \text{ \AA}$) and a few weak higher order reflections (see Fig. S3[†]).

The SAXS patterns of TNT, TP and TPT already contain these diffuse signals h_{π} , h_{ch} and the sharp reflection (10) in the pristine state at similar positions, revealing the development of the columnar structure from the beginning (see Fig. S4[†]). Consistently with the absence of mesophase observed by POM, the patterns of TN only show a blurred shoulder and a broad peak at the h_{π} and (10) locations, coming from facing mesogens and from loose piles separated by chains. Heating TP in the fluid state of the mesophase and subsequent cooling (see Fig. S4[†] and 3) sharpen and increase the number of visible small-angle reflections, impressively rising to six: (10), (11), (20), (21), (30), (22) (with q -ratios $1:\sqrt{3}:\sqrt{4}:\sqrt{7}:\sqrt{9}:\sqrt{12}$). The thermal treatment moreover leaves the location and shape of the h_{π} scattering unmodified (correlation length at 20 °C: $\zeta \approx 100 \text{ \AA}$, corresponding to *ca.* 30 mesogens) and thus restricts structural changes to a lateral rearrangement of columns consecutive to the fluidization of the aliphatic periphery. In TNT, the sharpening of the

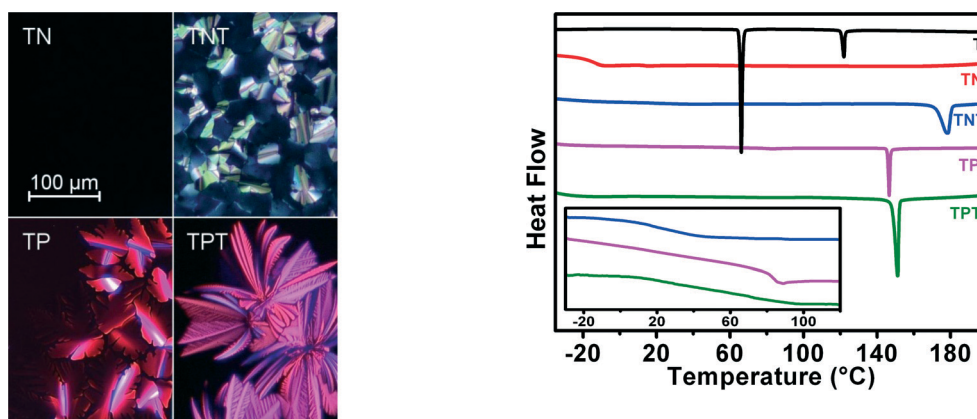


Fig. 2 POM textures (left) of TN in the isotropic liquid state at 20 °C, and of TNT, TP and TPT in the mesophase on cooling, at 100 °C, 135 °C and 150 °C, respectively; DSC traces (right) recorded during the second heating run at 5 °C min⁻¹ of T (hexakis(pentyloxy)-triphenylene), with melting and isotropization transitions at 65 °C and 121 °C, of TN, with a glass transition at –10 °C, of TNT, TP and TPT, with transitions to isotropic liquid at 173 °C, 146 °C and 159 °C, respectively. Inset view: DSC traces of the second heating run at 20 °C min⁻¹ of TNT, TP and TPT, with a glass-like transition between frozen and fluid states of the mesophase.

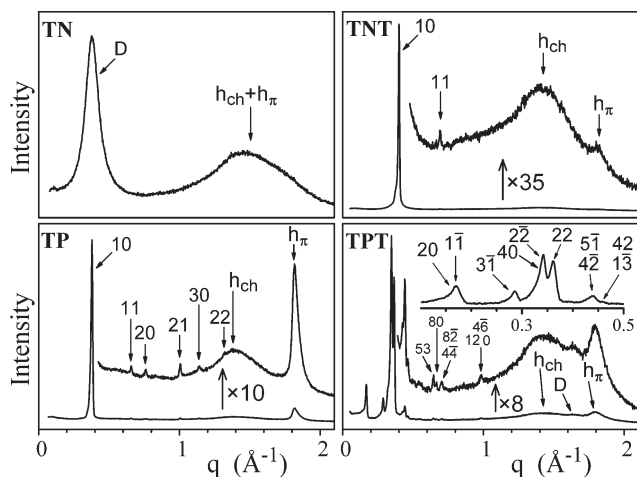


Fig. 3 SAXS patterns of triads/dyads TN, TNT, TP and TPT at room temperature, in the isotropic liquid (TN) or in frozen mesomorphic states (TNT, TP and TPT); curves on the top are zoomed to view weak signals; the inset view in the TPT graph is an additional pattern with a lower-angle SAXS line.

reflection (10) also proves the extension of the 2-dimensional lattice to a longer range, but at the cost of the widening of the h_π scattering ($\xi \approx 50$ Å) in combination with the appearance of only one higher order reflection. Hence the columnar stacking of TNT is less regular in the extended 2-dimensional lattice than the TP one. Finally, it should be stated that the 2-dimensional lattices of TNT and TP contain one single column; therefore the columns are composed of *a priori* undifferentiated triphenylene/naphthalene and triphenylene/perylene mesogenic stacks ($T_{\text{meso}}/N_{\text{meso}}$ and $T_{\text{meso}}/P_{\text{meso}}$).

In contrast, the elemental T and P units of TPT turned out to form distinct columns arranged in large lattices containing several molecular stacks of two T and one P columns separated by the aliphatic continuum. Differentiation of the col-

umn types in the pristine state is revealed by the doubling of the main peak around 18 Å and by the appearance of an additional reflection at double periodicity (see Fig. S4†). As for the TP dyad, the pristine TPT triad structure correlates to intermediate range and irreversibly transforms on first heating above the glass transition, in a long-correlated organization characterized by the appearance of numerous sharp reflections (see Fig. S5†). The π -stacking and the average section of individual T or P columns are hardly affected by the transformation, but the molecular stacks are rearranged in the lattice plane, resulting in a symmetry break to an oblique lattice (Col_{obl}) (see Table S2†). The Col_{obl} phase then is held up to the isotropization, directly recovered on cooling from the isotropic liquid and maintained on cooling in the frozen room temperature state, with only little variation of the lattice parameters with temperature. Small changes are nevertheless noticed in the frozen state, namely a slight re-broadening of the small-angle reflections (corresponding to roughly $\xi = 400$ Å) and the appearance of a weak wide-angle scattering maximum D (see Fig. 3). Such features most likely originate from the setting up of 3-dimensional correlations between mesogens from neighboring columns. All the meso-phase structural data are summarized in Table 2.

Description of bulk structures

Rylene diimide and triphenylene belong to the class of mesogens that self-organize by π -stacking and even show similar stacking distances.^{22,23} The different chemical natures and shapes of both types of mesogens make however their intimate mixing in stacks highly unlikely and in contrast, promote self-association in distinct columns. Consistently, structures with differentiated rylene diimide and triphenylene columns have recently been reported for other D–A triads;¹⁰ a new one has been observed for TPT which will be described now (see below).

Table 2 Mesomorphic structures and geometrical parameters of reference T ($N = 1$ mesogen per molecule), of dyads ($N = 2$) TN and TP, and of triads ($N = 3$) TNT and TPT, at temperature T (20 °C on cooling)

	T [°C]	Phase ^a	Parameters ^b
T	105	Col_{hex}	$a = 20.3$ Å; $A = 357$ Å ² ($Z = 1$); $h_\pi = 3.62$ Å ($\xi_\pi = 60$ Å) $S_{\text{col}} = 357$ Å ² ; $V_{\text{mol}} = 1276$ Å ³ ; $h_{\text{mol}} = 3.57$ Å
	65	Col_{hex}	$a = 20.3$ Å; $A = 356$ Å ² ($Z = 1$); $h_\pi = 3.49$ Å ($\xi_\pi = 120$ Å) $S_{\text{col}} = 356$ Å ² ; $V_{\text{mol}} = 1244$ Å ³ ; $h_{\text{mol}} = 3.49$ Å
TN	20	Iso	$D = 16.6$ Å ($\xi = 180$ Å); $\sigma_{\text{T/N}} = 290$ Å ² ; $V_{\text{mol}} = 1990$ Å ³ ; $H_{\text{mol}} = 3.4$ Å
TNT	140	Col_{hex}	$a = 18.5$ Å; $A = 297$ Å ² ($Z = 1/3$); $h_\pi = 3.53$ Å ($\xi_\pi = 25$ Å) $S_{\text{col}} = 297$ Å ² ; $V_{\text{mol}} = 3180$ Å ³ ; $h_{\text{mol}} = 3.58$ Å
	20	Col_{hex}	$a = 18.2$ Å; $A = 288$ Å ² ($Z = 1/3$); $h_\pi = 3.45$ Å ($\xi_\pi = 50$ Å) $S_{\text{col}} = 288$ Å ² ; $V_{\text{mol}} = 2920$ Å ³ ; $h_{\text{mol}} = 3.38$ Å
TP	140	Col_{hex}	$a = 19.6$ Å; $A = 334$ Å ² ($Z = 1/2$); $h_\pi = 3.52$ Å ($\xi_\pi = 40$ Å) $S_{\text{col}} = 334$ Å ² ; $V_{\text{mol}} = 2300$ Å ³ ; $h_{\text{mol}} = 3.45$ Å
	20	Col_{hex}	$a = 19.1$ Å; $A = 316$ Å ² ($Z = 1/2$); $h_\pi = 3.44$ Å ($\xi_\pi = 100$ Å) $S_{\text{col}} = 316$ Å ² ; $V_{\text{mol}} = 2110$ Å ³ ; $h_{\text{mol}} = 3.35$ Å
TPT	140	Col_{obl}	$a = 79.3$ Å; $b = 39.5$ Å; $\gamma = 92.9^\circ$; $A = 3120$ Å ² ($Z = 4$); $h_\pi = 3.61$ Å ($\xi_\pi = 20$ Å) $a/b = 2.01$; $S_{\text{col}} = 260$ Å ² ; $V_{\text{mol}} = 3350$ Å ³ ; $h_{\text{mol}} = 4.29$ Å
	20	Col_{obl}	$a = 75.3$ Å; $b = 40.5$ Å; $\gamma = 93.7^\circ$; $A = 3050$ Å ² ($Z = 4$); $h_\pi = 3.48$ Å ($\xi_\pi = 50$ Å) $a/b = 1.86$; $S_{\text{col}} = 254$ Å ² ; $V_{\text{mol}} = 3050$ Å ³ ; $h_{\text{mol}} = 4.01$ Å

^a Col_{hex} , Col_{obl} : hexagonal and oblique columnar mesophases; Iso: isotropic liquid. ^b Col_{hex} , Col_{obl} : a , b , γ , A (Z), h_π (ξ): 2-dimensional lattice parameters, lattice area and number of molecular stacks per lattice, π -stacking distance from the scattering maximum and correlation length (Scherrer); Iso: D (ξ), σ : lateral distance between mesogens from the peak maximum and correlation length, section of piled T/N units, according to $\sigma_{\text{T/N}} = (D/0.9763)^2$; ²¹ $S_{\text{col}} = A/(NZ)$: columnar cross-section; V_{mol} : molecular volume, directly measured for T or calculated from reference measurements for triads/dyads; $h_{\text{mol}} = (1/N)V_{\text{mol}}/S_{\text{col}}$: molecular slice thickness; $H_{\text{mol}} = (1/N)V_{\text{mol}}/\sigma_{\text{T/N}}$: piling distance.

The loss of differentiation in TP and TNT therefore excludes intimate mixing and is merely due to the permutation of entire groups of identical mesogens. Exchanges of entire columns between lattice nodes were reported for a previous system,²⁴ but this mechanism preserves the contrast between neighboring columns at local range and thus combines with the appearance of a diffuse superstructure signal not observed here. Hence different groups of stacked mesogens of the same nature alternate along the columnar axes. A lower limit for the mesogen group size can be derived from the correlation length ξ_π of the stacking (see Table 2), which basically lies in the few tens of mesogens range in the columnar phases and appears only slightly reduced with respect to the reference compound T: $\xi_\pi/h_\pi \approx 35$ mesogens for T at 65 °C, $\xi_\pi/h_\pi \approx 30$ mesogens for TP at 20 °C, $\xi_\pi/h_\pi \approx 15$ mesogens for TNT at 20 °C. Whatever the real average group size, their permutations between neighboring columns level out contrasts and shape anisotropies in the plane of the lattice without altering their long-range correlation, which ultimately leads to the observed hexagonal $P6mm$ arrangements of apparent undifferentiated columns (see Fig. 4). Both mesogens are therefore averaged to the same disc-shaped units of dimensions defined by the columnar section S_{col} and by the molecular slice thickness h_{mol} , obtained as the ratio of the half-dyad or third-triad volume and S_{col} . The accordance between h_{mol} and the π -stacking distances h_π confirmed the non-tilted stacking inside the columns inherited from the Col_{hex} phase of the reference compound T (see Table 2 and Fig. 5).

The local-range packing in the isotropic liquid phase of the non-mesomorphic dyad TN resembles a disordered modification of this Col_{hex} structure, within particular cross-sectional areas of piled T/N units $\sigma_{\text{T/N}}$ and piling distances H_{mol} close to S_{col} and h_{mol} in TNT (see Table 2 and Fig. 5).

The differences mainly come down to the shortened correlation lengths: the lateral packing of the T/N units only correlates over *ca.* ten units, the long-range orientational order has vanished and the π -stacking signal has flattened to a shoulder, revealing a very disordered piling.

The homogeneous aliphatic crown and the true disc-like shape of T_{meso} mesogens naturally promote hexagonal arrangements which persist in the TP dyad, *i.e.* after the intermingling of a stoichiometric amount of P_{meso} between T units. One might naively have expected that with only half the amount of P_{meso} , the Col_{hex} phase would also be preserved, but instead the TPT triad organizes in a Col_{obl} lattice including twelve columns. The reason is obviously that a specific structural feature (discussed hereafter) restores the differentiation between T and P columns and that the lattice therefore involves an integer number of triad stacks. The different cross-sectional shapes are restored at the same time and loom large constraints in the close packing of the lath-shaped P_{meso} (aspect ratio $\text{AR} \approx 1.5$) with disc-shaped T_{meso} ($\text{AR} = 1$), while the areas are, in contrast, close (see next part). These constraints certainly explain the appearance of a tilt-angle of mesogens within columns whereas T and PT form untilted mesophases. This angle of *ca.* 30° is directly determined from the ratio of the common stacking distance of mesogens, h_π , and of the slice thickness of the structure, h_{mol} (see Fig. 5), and mechanically leads to 15% shrinking of the lattice periodicities in the tilt directions.

The aspect ratio differences then get largely reduced when both mesogens tilt in different directions, *i.e.* toward long sides for P_{meso} and in the transverse direction for T_{meso} (Fig. 6). The tilt induction can, however, not compensate for the cross-sectional shapes and has no effect on other features determining the organization such as the end-on connected

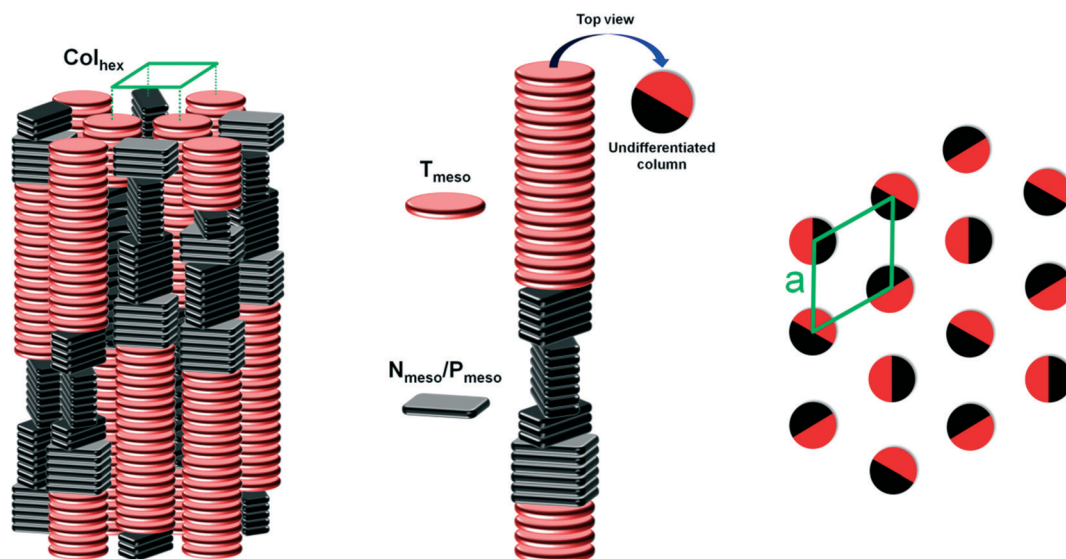


Fig. 4 Schematic view of the self-organization within the Col_{hex} mesophases of the TNT triad and TP dyad: left: entire groups of naphthalene or perylene diimide mesogens, N_{meso} or P_{meso} (black), and of triphenylene mesogens, T_{meso} (red), randomly alternate along and between columns; middle: mesogen groups superpose into unique undifferentiated $\text{N}_{\text{meso}}/\text{T}_{\text{meso}}$ or $\text{P}_{\text{meso}}/\text{T}_{\text{meso}}$ columns of average cylindrical cross-section; right: hexagonal $p6mm$ lattice (green lozenge) formed by undifferentiated columns.

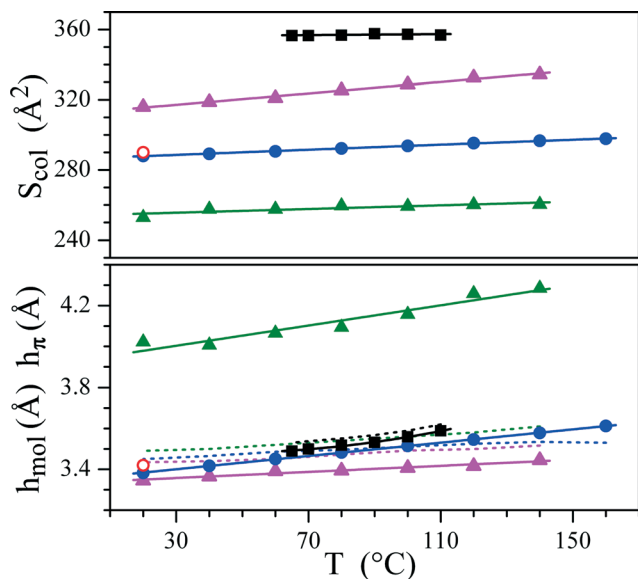


Fig. 5 Columnar cross-section S_{col} (top) and molecular slice thickness h_{mol} (bottom, symbols and solid lines) compared to the π -stacking distance from the scattering maximum h_{π} (dotted lines), as a function of temperature T , for triads/dyads TN (red open circles, $\sigma_{\text{T/N}}$ and H_{mol} instead of S_{col} and h_{mol} (see text)), TNT (blue lines and solid circles), TP (magenta lines and triangles), TPT (green lines and triangles), and for reference T (black lines and rectangles); lines are guides for the eyes.

spacers of the P_{meso} compared to the crown-like aliphatic periphery of the T_{meso} . During annealing in the fluid state, the twelve columns of the Col_{obl} lattice then develop as the optimal lateral arrangement of these unequal columns, for which schematic views based on symmetry, observed reflection series, geometrical parameters and molecular distances can be proposed (see Fig. 6). Conversely, the pristine state can be understood as an early stage of the same arrangement, in

which the orientation of the columnar cross-sections is only correlated over a few first neighbors.

In the fluid state of the Col_{hex} and Col_{obl} phases, the columns are largely free to slide along their axes relative to each other and the mesophases are therefore true 2-dimensional mesophases. This dynamics freezes in room temperature in the solid state, and short-range correlations appear between mesogen registries from neighboring columns in the Col_{obl} phase, resulting in a modified wide-angle scattering profile. In contrast, the mixed T/P columns of the Col_{hex} phase basically exclude such correlations and only freeze at the lattice nodes in the solid state, which improves the regularity of the 2-dimensional arrangement.

Discussion of the self-organization process

The self-organization type observed with these compounds basically differs from the lamello-columnar mesomorphism recently reported for other triads based on the same T-units linked to rylenes cores.¹⁰ The connection through short spacers in the previous triads (5 methylenes compared to 10 here) was found to promote the lamellar character of the molecular organization, which was moreover reinforced by the side-on connection and the comparable sizes of both moieties. In contrast, end-on connected rylenes cores self-assembled in layers would associate laterally through their short sides and therefore need to tilt by very large angles (60–65°) to equal the area imposed by the alternating rows of T columns. Such large tilt angles would strongly constrain the arrangement and moreover realize lesser efficient segregation with the aliphatic moieties, so that the entire surrounding of the rylenes columns by the aliphatic continuum and the formation of true columnar phases are finally preferable to the lateral association in layers.

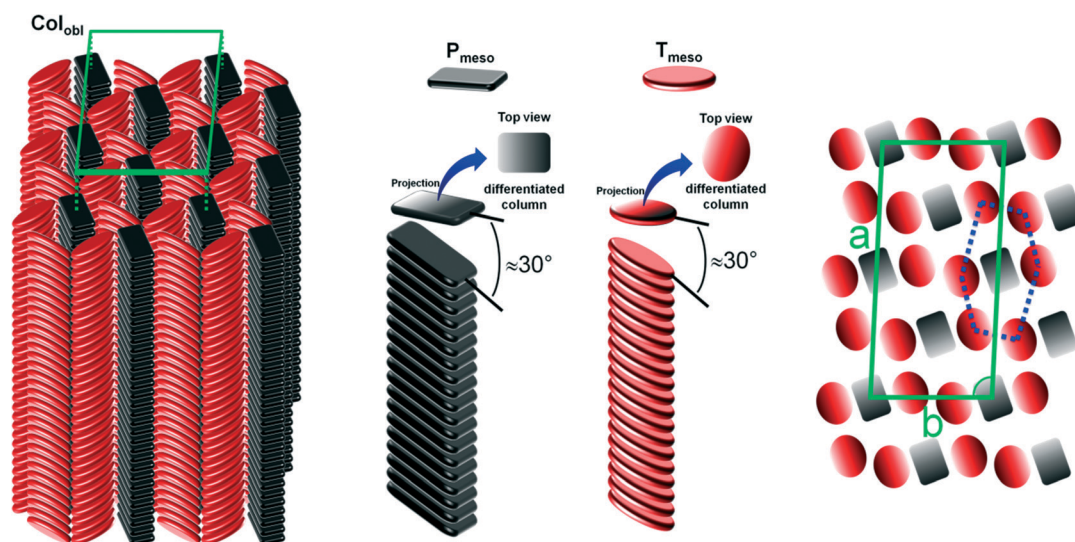


Fig. 6 Schematic view of the self-organization within the Col_{obl} mesophase of the TPT triad; middle: the P_{meso} and T_{meso} mesogens stack into differentiated columns with a tilt angle of ca. 30° reducing their projection in the lattice plane; right: possible arrangements within the plane of the oblique lattice (green frame); the blue dotted line defines a distorted honeycomb lattice formed by T units and surrounding the P units at the centers; the continuum of molten aliphatic chains fills the spaces between columns.

Various structures according to this template arise in the triad/dyad series, depending upon the ability of the individual compounds to preserve large groups of stacked mesogens and differentiated columns. Before deepening these aspects, the influence of the assembling process in the triad/dyad architecture and of the restricted molecular diffusion should be considered, for which the comparison of T and its dimer TT might be a pertinent reference. The isotropization temperature of the dimer was actually shown to lie 14 °C above that of the monomer (e.g. T), but the mesophase structure was identical and the melting transition did not move significantly.²⁰ In analogy with a previous work, a portion of the isotropization temperature increase noticed for TNT, TPT and TP might originate from the general architecture, but the other self-organization features are likely due to the association/connection of the different mesogens.

The most remarkable aspect is maybe the different effects of the rylene proportion on both cores: the TNT triad shows a Col_{hex} phase as the reference T and with even the highest isotropization temperature of the series, but the mesomorphism vanishes with the increase of the N_{meso} proportion to 1:1 (TN dyad). In contrast, the Col_{hex} phase reappears for the highest P_{meso} proportion (TP dyad), while the intermediate TPT triad exhibits a Col_{obl} phase. Yet N_{meso} and P_{meso} are clearly similar considering their chemical nature, lateral interactions and segregation power with respect to the alkyl chains and to other mesogens. Their principal difference is actually their size, which requires to be compared to T_{meso} to understand the potential role of this characteristic on the self-organization. For this purpose, T was compared to two analogous reference compounds, P and N, with the corresponding rylene mesogen and aliphatic peripheries equivalent to the one of T. These new references are non-mesomorphic, but the volumes can accurately be compared in the isotropic liquid phase, from which the volume in the mesophases deviate by less than one percent (see Fig. 7). After subtraction of the alkyl chain contribution, it appears that mesogens N_{meso} and P_{meso} have volumes 30% below and 5% above T_{meso}, respectively. Considering the similar stacking distances h_{π} found for all compounds at the same temperatures, (see Fig. 5), the mesogen sections lie in the same ratios as the volumes, thus for $h_{\pi} \approx 3.45 \text{ \AA}$ at room temperature: $S_{N_{\text{meso}}} = 84$, $S_{P_{\text{meso}}} = 121$, $S_{T_{\text{meso}}} = 116 \text{ \AA}^2$.

As discussed above, the 2:1 stoichiometry of the triads is intrinsically favorable to differentiation, since the major component can occupy the nodes of the (regular or distorted) honeycomb lattice and the minor component, the centers of the hexagonal cells. The circumscribed area at the centers is however identical to the area at the honeycomb lattice nodes and the formation of a regular structure therefore requires that both components have approximately the same cross-sectional area. This is obviously the case for the T_{meso}/P_{meso} couple and differentiation therefore spontaneously appears for TPT. The smaller size of N_{meso} in contrast prevents the formation of a regular honeycomb lattice in TNT. This could have resulted in an amorphous state with segregation from

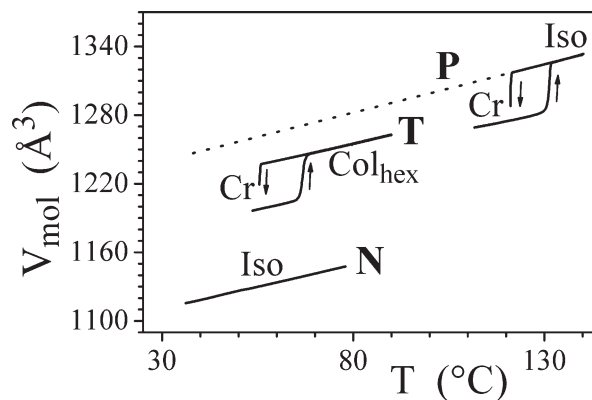


Fig. 7 Molecular volumes of reference compounds T (hexakis(pentyloxy)-triphenylene), N (*N,N'*-di(pentadecan-8-yl)-naphthalene-diimide) and P (*N,N'*-di(pentadecan-8-yl)-perylene-diimide) measured versus temperature by dilatometry; Cr: crystal phase; Col_{hex}: hexagonal columnar mesophase; Iso: isotropic liquid; dotted line: extrapolation; for the complete experimental curve of T, extending to the isotropic liquid phase, see Fig. S6†

aliphatic chains and differentiation of columns limited to local range. Instead, it turned out preferable to maintain the long-range correlated lattice and lose the differentiation. Hence the distribution of groups of identical mesogens over all columns yielded the single-column Col_{hex} phase.

The three columns per elementary hexagonal cell (two for the distorted honeycomb and one for the centers) prevent any separation of column types under the conditions of 1:1 stoichiometry. Long-range differentiation should therefore not occur in the dyads, but still could be preserved at the local range, which is indeed observed for TP. In this way, T_{meso} and P_{meso} remain separated in different groups over the correlation length of the stacking, but at a larger distance, the equivalence of the lattice nodes imposed by the stoichiometry just results in the random distribution of groups in the lattice and in the related symmetry elevation to Col_{hex}. The same organization appears with N_{meso} already for the triad, but in relation to its small size hampering the insertion between six neighboring T columns. The 2:1 stoichiometry promotes long-range honeycomb lattices and relaxes these steric constraints through frequent alternation of the mesogen nature at the lattice nodes. This averaging effect however vanishes in the dyad and the irregular environment of the N_{meso} groups looms large, which ends up with a strongly disordered piling and the disappearance of the mesomorphism, likely in relation to a more intimate mixing of both mesogens.

Spontaneous alignment in thin films

Applications of organic semiconducting materials often require thin films with controlled morphology.^{7c} When these materials exhibit mesophases, the film preparation is facilitated by the long-range orientational order combined with the fluidity and the self-healing ability against structural defects inherent to mesomorphism.^{6b,c} In addition, the association of different mesogens in the triad/dyad architectures

strongly hampers the crystallization and the structures forming at higher temperature just freeze on cooling at room temperature.¹⁰ Our triad/dyads meet these requirements: they link recognized semiconducting units, most show mesomorphism and none does crystallize, which opens up possibilities to freeze morphologies having been obtained in the fluid state of mesophases and limiting the grain boundary formation. The results depend on the architecture but also on the type of mesophase, which is addressed hereafter for the mesomorphous triad/dyad pair TPT/TP.

For this purpose, tens of nanometer scale films of the TP dyad were deposited by spin-coating on top of a silicon wafer from chloroform solutions. The GIXS patterns of the as prepared films prove the self-organization behaviour, which is identical to the pristine bulk structure, namely a Col_{hex} phase of undifferentiated T/P columns (see Fig. S7†). As revealed by the unique broadened signal, the organization involves a lot of disorder, in relation to the frozen state at the deposition temperature (room temperature) and with the fast deposition technique. Surprisingly, the domains turned out to be spontaneously oriented at this stage of the preparation. Consistent with previous findings for classical discotic systems,²⁵ this spontaneous orientation consists of planar lying column rows, as demonstrated by the splitting of the first order reflection in spots at 0° and ±60° from the meridian and by the

h_π scattering located at the equator. The annealing step in the fluid state of the mesophase logically does not modify this already optimal orientation, but develops the long-range order similarly to that in the bulk. The appearance of numerous sharp dots corresponding to higher order reflections then attests to the regularity of the structure and to the nearly perfect planar orientation (see Fig. 8, top left). Films prepared by the same procedure and studied using tapping mode atomic force microscopy (AFM) appear relatively uniform before thermal treatment, with no specific nanostructures and with roughness less than 1 nm (see Fig. S9†). After their annealing in the fluid state of the mesophase, the films become clearly nanostructured, with terraces of 1.7 nm or of multiples of 1.7 nm height (see Fig. 8 top right). This height coincides with the inter-row spacing d_{10} from the SAXS patterns, in agreement with the planar orientation of the columns evidenced in the GIXS patterns.

In the highly symmetric Col_{hex} structure of TP, the surface alignment of the {10} planes turned out to be preferred over the alternative alignment of the lattice plane, which means that the interactions at the interfaces favor an edge-on orientation of the mesogens over face-on. TPT is constituted by the same mesogens and should thus also lead to lying column alignments in the mesophase. This was indeed verified in some patterns showing an intense h_π scattering on the equator

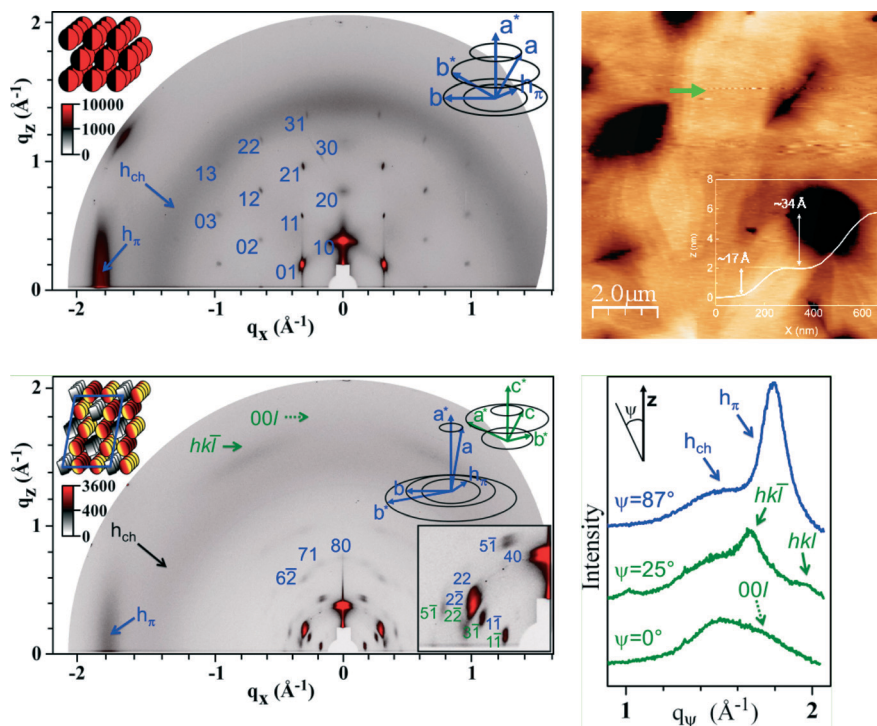


Fig. 8 Top: GIXS pattern (left) compared to topography AFM image in tapping mode (right) of thin films of dyad TP, spin-coated on silicon wafer and annealed at 120 °C for 2 hours in vacuum; inset views: alignment of mixed T/P columns (red & black discs) on top of the substrate (lying columns), orientation of the crystallographic axes (blue) and height profile (the green arrow in the AFM image shows the profile direction). Bottom: GIXS pattern of the TPT triad (left), dip-coated on silicon wafer and annealed at 120 °C for 2 hours in vacuum; inset views: alignment of tilted T and P columns (yellow-red and grey shaded) in the Col_{obt} phase on top of the substrate (lying columns), corresponding orientation of the crystallographic axes (blue) and orientation of the crystallographic axes for crystal-like domains (green); profiles of GIXS pattern (right) within sectors $\psi \pm 3^\circ$, for azimuthal angles $\psi = 0^\circ, 25^\circ$, and 87° (origin on the meridian).

beside the molten chain ring (see Fig. 8, bottom). The small-angle spots related to the same mesophase moreover confirm the arrangement in the Col_{obl} lattice, with the alignment of the a^* -axis on the meridian and a somewhat smaller elongation with respect to the bulk structure ($a \approx 70 \text{ \AA}$, $b \approx 45 \text{ \AA}$; $\gamma = 98 \pm 3^\circ$). In coexistence with the major Col_{obl} fraction, the film contains domains of another phase for which the stacking direction flips to the surface normal and the corresponding scattering signal splits in semi-diffuse bows lying close to the meridian. This indicates the appearance of $(00l)/(hk\bar{l})/(hkl)$ reflections from a 3-dimensional phase, with crystalline order and still molten alkyl chains. Depending on the conditions of film preparation, the Col_{obl} domains even nearly vanished and were replaced by further crystalline-like states, whose investigation would have required additional measurements and is beyond the scope of the contribution (see example in Fig. S8†).

The occurrence of these crystal-like states in the films complicates obtaining of the uniform lying column alignments desired for the investigation of semiconducting properties. The achievement of this goal might however only be a matter of process optimization since the films already contain variable amounts of aligned Col_{obl} domains and since the organization in the bulk was shown to freeze above room temperature. Further trials and the resort to more sophisticated techniques combining in-plane alignment and surface-induced alignment are indeed justified by the differentiation of the P and T columns in the mesophase and the possible ambipolar properties of the final material.

Conclusion

A new series of liquid crystalline D–A dyads and D–A–D triads based on triphenylene and rylene diimide cores as donor (D) and acceptor units (A), respectively, both entities being linked by alkyl chain spacers, have been successfully designed, synthesized and characterized. In solution, the HOMO/LUMO values of the individual D/A cores turn out to be preserved in the multiads. In the solid state, the linker authorizes the stacking in individual columns, isolated from each other by molten chains. One of these molecules effectively shows self-organization in a genuine columnar mesophase with the optimally intermingled arrangement of differentiated D and A columns. In contrast, the three other molecules give rise to mixed D/A columns or even to amorphous states, and geometrical assembling rules for the appropriate molecular design could subsequently be derived. The coveted structure of distinct columns appears indeed in conjunction with the 2 : 1 stoichiometry of the triad, compatible with the honeycomb arrangements, and with the size-compatibility of mesogens, realized for the perylene diimide/triphenylene couple. The unfavorable 1 : 1 stoichiometry of the dyad architecture or the substitution of perylene diimide by the smaller naphthalene diimide leads to a columnar phase with mixed columns or even to the vanishing of the mesomorphism when both unfavorable features were combined. This comprehensive study

eventually shows that by relevant chemical engineering it is possible to control the nanostructuring of D–A discotic multiads to give rise to differentiated D and A columnar arrangements. Since such molecular organizations provide the ideal configuration for 1D hole and electron transport and are highly desirable for potential semiconducting applications, this work opens up promising opportunities for the elaboration of ambipolar devices and, more widely, for optoelectronic applications.

Acknowledgements

This work has been supported by the French National Agency (ANR) in the frame of its program in Nanosciences and Nanotechnologies (TRAMBIPOLY project ANR-08-NANO-051). Y. Xiao and X. Su thank the China Scholarship Council, Ministry of Education, People's Republic of China. We thank the Pohang Accelerator Laboratory (PAL) for giving us the opportunity to perform the GIXS measurements, MEST and POSTECH for supporting these experiments, Drs. Tae Joo Shin and Hyungju Ahn for adjustments and help, and other colleagues from the 9A USAXS beamline for assistance. This research was supported by the Leading Foreign Research Institute Recruitment Program through the National Research Foundation of Korea (NRF) funded by the Ministry of Science, ICT & Future Planning (NRF-2010-00453). The authors also acknowledge the International Research Network (GDRI, CNRS) on "Functional Materials for Organic Optics, Electronics and Devices" (FUNMOOD).

References

- (a) S. R. Forrest, *Nature*, 2004, **428**, 911–918; (b) C. Wang, H. Dong, W. Hu, Y. Liu and D. Zhu, *Chem. Rev.*, 2012, **112**, 2208–2267.
- (a) L. Dong, W. Li and W.-S. Li, *Nanoscale*, 2011, **3**, 3447–3461; (b) M. Wang and F. Wudl, *J. Mater. Chem.*, 2012, **22**, 2429–24314; (c) L. F. Dössel, V. Kamm, I. A. Howard, F. Laquai, W. Pisula, X. Feng, C. Li, M. Takase, T. Kudernac, S. de Feyter and K. Müllen, *J. Am. Chem. Soc.*, 2012, **134**, 5876–5886; (d) J. M. Mativetsky, M. Kastler, R. C. Savage, D. Gentilini, M. Palma, W. Pisula, K. Müllen and P. Samori, *Adv. Funct. Mater.*, 2009, **19**, 2486–2494; (e) R. Charvet, Y. Yamamoto, T. Sasaki, J. Kim, K. Kato, M. Takata, A. Saeki, S. Seki and T. Aida, *J. Am. Chem. Soc.*, 2012, **134**, 2524–2527; (f) D. Zeng, I. Tahar-Djebbar, Y. Xiao, F. Kameche, N. Kayunkid, M. Brinkmann, D. Guillon, B. Heinrich, B. Donnio, D. A. Ivanov, E. Lacaze, D. Kreher, F. Mathevet and A.-J. Attias, *Macromolecules*, 2014, **47**, 1715–1731; (g) R. A. Segalman, B. McCulloch, S. Kirmayer and J. J. Urban, *Macromolecules*, 2009, **42**, 9205–9216; (h) S. Huettner, M. Sommer, J. Hodgkiss, P. Kohn, T. Thurn-Albrecht, R. H. Friend, U. Steiner and M. Thelakktat, *ACS Nano*, 2011, **5**, 3506–3515.
- (a) M. Sommer, A. S. Lang and M. Thelakktat, *Angew. Chem., Int. Ed.*, 2008, **47**, 7901–7904; (b) S.-Y. Ku, M. A. Brady, N. D.

- Treat, J. E. Cochran, M. J. Robb, E. J. Kramer, M. L. Chabinyk and C. J. Hawker, *J. Am. Chem. Soc.*, 2012, **134**, 16040–16046.
- 4 (a) H. Hayashi, W. Nishihashi, T. Umeyama, Y. Matano, S. Seki, Y. Shimizu and H. Imahori, *J. Am. Chem. Soc.*, 2011, **133**, 10736–10739; (b) L. Bu, X. Guo, B. Yu, Y. Qu, Z. Xie, D. Yan, Y. Geng and F. Wang, *J. Am. Chem. Soc.*, 2009, **131**, 13242–13243; (c) X. Kong, Z. He, Y. Zhang, L. Mu, C. Liang, B. Chen, X. Jing and A. N. Cammidge, *Org. Lett.*, 2011, **13**, 764–767; (d) P.-O. Schwartz, L. Biniek, E. Zaborova, B. Heinrich, M. Brinkmann, N. Leclerc and S. Mery, *J. Am. Chem. Soc.*, 2014, **136**, 5981–5992; (e) S. K. Gupta, S. Setia, S. Sidiq, M. Gupta, S. Kumar and S. K. Pal, *RSC Adv.*, 2013, **3**, 12060–12065; (f) E. Beltran, M. Garzoni, B. Feringan, A. Vancheri, J. Barbera, J. L. Serrano, G. M. Pavan, R. Gimenez and T. Sierra, *Chem. Commun.*, 2015, **51**, 1811–1814; (g) K. J. Lee, J. H. Woo, E. Kim, Y. Xiao, X. Su, L. M. Mazur, A.-J. Attias, F. Fages, O. Cregut, A. Barsella, F. Mathevet, L. Mager, J. W. Wu, A. D'Aléo and J.-C. Ribierre, *Phys. Chem. Chem. Phys.*, 2016, **18**, 7875–7887.
- 5 *Handbook of Liquid Crystals*, ed. J. W. Goodby, P. J. Collings, T. Kato, C. Tschierske, H. F. Gleeson and P. Raynes, Wiley-VCH, Weinheim, Germany, 2nd edn, 2014.
- 6 (a) M. O'Neill and S. M. Kelly, *Adv. Mater.*, 2011, **23**, 566–584; (b) F. Lincker, A.-J. Attias, F. Mathevet, B. Heinrich, B. Donnio, J.-L. Fave, P. Rannou and R. Demadrille, *Chem. Commun.*, 2012, **48**, 3209–3211; (c) L. Mazur, A. Castiglione, K. Ocytko, F. Kameche, R. Macabies, A. Ainsebaa, D. Kreher, B. Heinrich, B. Donnio, S. Sanaur, E. Lacaze, J.-L. Fave, K. Matczyszyn, M. Samoc, J. W. Wu, A.-J. Attias, J.-C. Ribierre and F. Mathevet, *Org. Electron.*, 2014, **15**, 943–953; (d) W. Pisula, M. Zorn, J. C. Young, K. Müllen and R. Zentel, *Macromol. Rapid Commun.*, 2009, **30**, 1179–1202; (e) Y. Shimizu, K. Oikawa, K. Nakayama and D. Guillon, *J. Mater. Chem.*, 2007, **17**, 4223–4229; (f) M. Funahashi, *J. Mater. Chem. C*, 2014, **2**, 7451–7459; (g) Y. Geng, S. Chang, K. Zhao, Q. Zeng and C. Wang, *J. Phys. Chem. C*, 2015, **119**, 18216–18220; (h) H. Iino, T. Usui and J. Hanna, *Nat. Commun.*, 2015, **6**, 6828.
- 7 (a) S. Chandrasekhar, B. K. Sadashiva and K. A. Suresh, *Pramana*, 1977, **9**, 471–480; (b) S. Kumar, *Chem. Soc. Rev.*, 2006, **35**, 83–109; (c) S. Sergeev, W. Pisula and Y. H. Geerts, *Chem. Soc. Rev.*, 2007, **36**(12), 1902–1929; (d) B. R. Kaafarani, *Chem. Mater.*, 2011, **23**, 378–396; (e) T. Wöhrle, I. Wurzbach, J. Kirres, A. Kostidou, N. Kapernaum, J. Litterscheidt, J. C. Haenle, P. Staffeld, A. Baro, F. Giesselmann and S. Laschat, *Chem. Rev.*, 2016, **116**, 1139–1241.
- 8 (a) D. Adam, P. Schumacher, J. Simmerer, L. Hausling, K. Siemensmeyer, K. H. Etbach, H. Ringsdorf and D. Haarer, *Nature*, 1994, **371**, 141; (b) H. Iino, Y. Takayashiki, J. Hanna, R. J. Bushby and D. Haarer, *Appl. Phys. Lett.*, 2005, **87**, 192105; (c) H. Iino, J. Hanna, R. J. Bushby, B. Movaghar and B. J. Whitaker, *Appl. Phys. Lett.*, 2006, **100**, 043716; (d) Yasuo Miyake, B. A. Fujiib, M. Ozakib and Y. Shimizu, *Synth. Met.*, 2009, **159**, 875–879; (e) N. Mizoshita, H. Monobe, M. Inoue, M. Ukon, T. Watanabe, Y. Shimizu, K. Hanabusa and T. Kato, *Chem. Commun.*, 2002, 428–429; (f) P. Staffeld, M. Kaller, S. J. Beardsworth, K. Tremel, S. Ludwigs, S. Laschat and F. Giesselmann, *J. Mater. Chem. C*, 2013, **1**, 892–901.
- 9 (a) X. Zhan, A. Facchetti, S. Barlow, T. J. Marks, M. A. Ratner, M. R. Wasielewski and S. R. Marder, *Adv. Mater.*, 2011, **23**, 268–284; (b) S. Alibert-Fouet, I. Seguy, J.-F. Bobo, P. Destruel and H. Bock, *Chem. – Eur. J.*, 2007, **13**, 1746–1753; (c) C. Li and H. Wonneberger, *Adv. Mater.*, 2012, **24**, 613–636; (d) Z. Anl, J. Yu, S. C. Jones, S. Barlow, S. Yoo, B. Domercq, P. Prins, L. D. A. Siebbeles, B. Kippelen and S. R. Marder, *Adv. Mater.*, 2005, **17**, 2580–2583; (e) M. Funahashi and A. Sonoda, *J. Mater. Chem.*, 2012, **22**, 25190–25197; (f) F. Würthner, C. R. Saha-Möller, B. Fimmel, S. Ogi, P. Leowanawat and D. Schmidt, *Chem. Rev.*, 2016, **116**, 962–1052.
- 10 K.-Q. Zhao, L.-L. An, X.-B. Zhang, W.-H. Yu, P. Hu, B.-Q. Wang, J. Xu, Q.-D. Zeng, H. Monobe, Y. Shimizu, B. Heinrich and B. Donnio, *Chem. – Eur. J.*, 2015, **21**, 10379–10390.
- 11 W. Kreuder, H. Ringsdorf, O. Herrmann-Schönherr and J. H. Wendorff, *Angew. Chem., Int. Ed. Engl.*, 1987, **26**, 1249–1252.
- 12 X. Kong, Z. He, H. Gopee, X. Jing and A. N. Cammidge, *Tetrahedron Lett.*, 2011, **52**, 77–79.
- 13 A. Wicklein, A. Lang, M. Muth and M. Thelakkat, *J. Am. Chem. Soc.*, 2009, **131**, 14442–14453.
- 14 F. Würthner, C. Thalacker, S. Diele and C. Tschierske, *Chem. – Eur. J.*, 2001, **7**, 2245–2253.
- 15 N. Boden, R. C. Borner, J. Bushby, A. N. Cammidge and M. V. Jesudason, *Liq. Cryst.*, 1993, **15**(6), 851–858.
- 16 H. Langhals and S. Kinzel, *J. Org. Chem.*, 2010, **75**, 7781–7784.
- 17 (a) J. L. Bredas, R. Silbey, D. S. Boudreaux and R. R. Chance, *J. Am. Chem. Soc.*, 1983, **105**, 6555–6559; (b) M. Thelakkat and H. Schmidt, *Adv. Mater.*, 1998, **10**, 219–223; (c) P. Bauer, H. Wietasch, S. M. Lindner and M. Thelakkat, *Chem. Mater.*, 2007, **19**, 88–94.
- 18 I. Seguy, P. Jolinat, P. Destruel, J. Farenc, R. Mamy, H. Bock, J. Ip and T. P. Nguyen, *J. Appl. Phys.*, 2001, **89**, 5442–5448.
- 19 L. E. Polander, S. P. Tiwari, L. Pandey, B. M. Seifried, Q. Zhang, S. Barlow, C. Risko, J.-L. Bredas, B. Kippelen and S. R. Marder, *Chem. Mater.*, 2011, **23**, 3408–3410.
- 20 S. Zamir, R. Poupko, Z. Luz, J. B. Hiker, C. Boeffel and H. Zimmermann, *J. Am. Chem. Soc.*, 1994, **116**, 1973–1980.
- 21 M. Marcos, R. Giménez, J. L. Serrano, B. Donnio, B. Heinrich and D. Guillon, *Chem. – Eur. J.*, 2001, **7**, 1006–1013.
- 22 C. W. Struijk, A. B. Sieval, J. E. J. Dakhorst, M. van Dijk, P. Kimkes, R. B. M. Koehorst, H. Donker, T. J. Schaafsma, S. J. Picken, A. M. van de Craats, J. M. Warman, H. Zuilhof and E. J. R. Sudholter, *J. Am. Chem. Soc.*, 2000, **122**, 11057–11066.
- 23 S. Kumar, *Liq. Cryst.*, 2004, **31**, 1037–1059.
- 24 I. Bury, B. Heinrich, C. Bourgogne, G. H. Mehl, D. Guillon and B. Donnio, *New J. Chem.*, 2012, **36**, 452–468.
- 25 A. Tracz, J. K. Jeszka, M. D. Watson, W. Pisula, K. Müllen and T. Pakula, *J. Am. Chem. Soc.*, 2003, **125**, 1682–1683.